Journal of Applied Polymer Science

Polyaniline with High Crystallinity Degree: Synthesis, Structure, and Electrochemical Properties

Xianfeng Du, Youlong Xu, Lilong Xiong, Yang Bai, Jianbo Zhu, Shengchun Mao
Electronic Materials Research Laboratory, Key laboratory of the Ministry of Education & International Center of Dielectric Research, Department of Electronic Science and Technology, Xi'an Jiaotong University, Xi'an 710049, People's Republic of China
Correspondence to: Y. Xu (E-mail: ylxu@mail.xjtu.edu.cn)

ABSTRACT: Polyaniline (PANI) with high crystallinity degree was facilely synthesized on the surface of stainless steel net by galvanostatic method. The effect of polymerization current density on the characteristics of morphology and structure had been investigated by field emission scanning electron microscopy (FE-SEM), Fourier transforms infrared (FTIR), X-ray photoelectron spectroscopy (XPS), and X-ray diffraction (XRD). FE-SEM observations disclosed that PANI was deposited as nanofibers and their diameters decreased with the polymerization current density. FTIR studies revealed that degree of oxidation increased in order PANI-2 < PANI-6 < PANI-10. XPS measurements displayed that PANI polymerized at 6 mA cm^{-2} (PANI-6) exhibited much higher doping level of 77.8%, which favored the conductivity. XRD analysis discovered that the obtained PANI showed high crystallinity degree in which PANI-6 possessed highest crystallinity degree (X_{cr}) up to 67%. Electrochemical performances of PANI as electrode materials were studied via cyclic voltammetry. The results presented that PANI-6 possessed greater discharge capacity and better reversibility. © 2014 Wiley Periodicals, Inc. J. Appl. Polym. Sci. **2014**, *131*, 40827.

KEYWORDS: conducting polymers; crystallization; electrochemistry; structure-property relations; synthesis and processing

Received 18 December 2013; accepted 6 April 2014
DOI: 10.1002/app.40827

INTRODUCTION

Polyaniline (PANI) as a representative conductivity polymer has attracted huge interest of researchers owing to its excellent electronical, optical, thermoelectric, and electrochemical properties in the last decade. PANI has been successfully applied in new advanced materials for antistatic protection, photovoltaics, thermoelectric energy conversion, supercapacitor, lithium ion battery, and so forth.[1–5]

Generally, PANI can be synthesized by chemical polymerization in solution in the form of power or electrochemical polymerization as a film on the electrode surface.[6–8] For chemical polymerization, it is an inexpensive and facile way. However, the residue surfactants and oxidants used possibly degrade the sample's properties. Electrochemical polymerization is considered as a more environmental benign way to fabricate PANI with better properties because no surfactants and oxidants are needed.

Various electrochemical methods, such as potentiostatic,[9] galvanostatic,[10] or cyclic voltammetry (CV)[11] means, have been applied in the preparation of PANI. Most of the researchers paid more attention on the properties of PANI instead of the structure inasmuch as PANI obtained was usually amorphous or got much low crystallinity degree. The performances of PANI, nevertheless, directly depend on its structure. Consequently, elucidation of the relationships between its properties and chain structure is extremely important.[8,12,13] Some investigations in this case have been carried out and gained great knowledge,[14–19] whereas their studies based on the fact that the synthesized PANI did not exhibit very high crystallinity. To the best of the author's knowledge, there is no report about this so far. Therefore, the fact that how to obtain PANI with high crystallinity degree becomes an important issue that needs to be addressed.

In this study, PANI with high crystallinity degree was synthesized by galvanostatic method on the basis of several points of view: the production is purer and more homogeneous, the devices are facile, and different thickness films could be obtained by controlling polymerization time and/or current density. The data about its spectral properties, structure, conductivity, and electrochemical properties were presented. The effect of polymerization current density on the structure, degree of oxidation (DO), doping level (DL), and crystallinity degree was investigated. The relationship between structure and electric properties was discussed.

EXPERIMENTAL

Reagents

Aniline (C_6H_7N, analytical grade from Xi'an Chemical Industry, China) was distilled under reduced pressure before use.

Analytical grade reagent, perchloric acid ($HClO_4$, Xi'an Chemical Industry, China) as the dopant was used without further purification. The stainless steel net was employed as support and polished by $HClO_4$ before polymerization. In this study, all solutions were prepared from deionized (DI) water produced by Milli-Q-Reference water system (Millipore, Bedford, MA). The aniline solution was freshly prepared by adding 0.5*M* of aniline to 2*M* of $HClO_4$ solution.

Synthesis of PANI Samples

The samples of PANI were synthesized via galvanostatic method with VMP2 multichannel potentiostat (Princeton Applied Research, USA), and potential data were recorded simultaneously. The stainless steel nets were immersed into the aniline solution, act as working electrode and counter electrode. The reference electrode was saturated calomel electrode (SCE) (Model 232, Shanghai Ruosull Technology, China). When loaded 2, 6, and 10 mA cm^{-2} of current density, PANI films were electrodeposited on the surface of stainless steel nets, marked as PANI-2, PANI-6, and PANI-10, respectively. Then, the films were washed with DI water and 2*M* of $HClO_4$ solution, respectively, and finally dried at 60°C for 24 h in a vacuum oven. Some of these films were scraped off from the nets for characterizations.

Characterization

The morphology of PANI was characterized by field emission scanning electron microscopy (FE-SEM), Quanta 250FEG (FEI, USA) operated at 10 kV. Fourier transforms infrared (FTIR) measurements of the obtained PANI samples in the range of 400–4000 cm^{-1} were registered by a fully computer-controlled Avatar 360 FTIR ESP (Thermo Nicolet, USA) with a resolution of 2 cm^{-1}. Measurements were carried out *ex situ* in the transmission mode as KBr tables. The surface composition and elemental chemical state of the samples were examined by X-ray photoelectron spectroscopy (XPS) using an Escalab Mk II (VG Scientific, United Kingdom) apparatus with an MgKα X-ray source (photons, 1468.3 ev). All samples in film form were mounted on standard sample holders by means of double-sided adhesive tapes. The X-ray source was run at 15.5 KV and 20 mA. Pressure in the analysis chamber during the examinations was typically 10^{-8} mbar or below. All core level spectra were referenced to the C1s peak of PANI at 283.1 ev. The structure of the different samples was performed by wide-angle X-ray diffractograms on a computerized X-ray diffraction (XRD) system, Rigaku D/MAX-2400 (Rigaku, Japan). Cu K_α radiation ($\lambda = 1.54187$ Å) was monochromatized by a Ni-filter pulse-height analyzer and registered with a scintillation counter. Diffractograms were carried out in 2θ scan model in the range of 10–60° with an accuracy of 0.05°.

The specific conductivity of obtained PANI samples was measured using a four-probe setup (Model SDY-4, Guangzhou Semiconductor Material Academe, China) at ambient temperature. The ohmic character of the contacts with tablets of the PANI samples was achieved by the gold plating of the probe tips. Cyclic voltammograms of PANI films were recorded using VMP2 multichannel potentiostat under the synthesis condition except that the solution did not contain aniline. The scanning potential range is from −0.2 to 1.0 V versus SCE with a scanning rate of 1 mV s^{-1}.

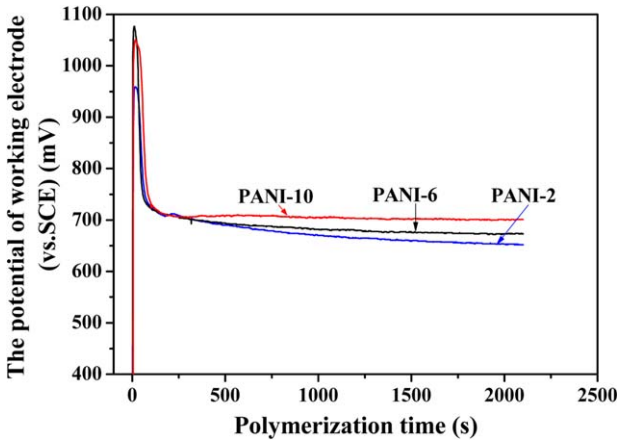

Figure 1. Curves of the polymerization potential versus polymerization time at 2, 6, and 10 mA cm^{-2}. [Color figure can be viewed in the online issue, which is available at wileyonlinelibrary.com.]

RESULTS AND DISCUSSION

Galvanostatic Polymerization

The curves of potential–time transients traced during the galvanostatic electrodeposition are shown in Figure 1. There are three steps during all polymerization processes. The first step corresponds to the anodic passivation of the stainless steel,[9] which leads to a sharp increase in the potential. The second step is related to nucleation and growth of PANI on the surface of the stainless steel.[20] Once PANI is formed, the potential rapidly decreases because of the self-catalyzing of PANI which makes polymerization become easier.[21,22] When the surface of stainless steel is fully covered by PANI, the potential decreases slowly to a steady state, which is the third step.[23] As shown in Figure 1, it is clearly shown that the potentials at steady state are different under various polymerization current densities. In this study, they are ~650, 680, and 700 mV (vs. SCE) at 2, 6, and 10 mA cm^{-2}, respectively. They increase with current density, as it is partially caused by anodic polarization. The higher the current density is, the greater the polarization potential is. The PANIs synthesized during this potential range get emeraldine structure.[24]

Morphological Properties

Figure 2 shows the surface morphology of PANI synthesized at different current densities. It can be seen that all samples are porous and composed of nanofibers. The quantity of these nanofibers increases, whereas their diameter decreases, with polymerization current density. This can be explained as follows: aniline is easier to be oxidized into radical cations at higher potential caused by larger current density, resulting in more nuclei, which will grow to nanofibers during the next polymerization. As shown in Figure 2, it is also clear that the pore size of PANI-2 is much larger than PANI-6 and PANI-10. Therefore, it can be evolved that PANI-6 and PANI-10 have much larger specific surface area than that of PANI-2, which will promote their electrochemical properties.

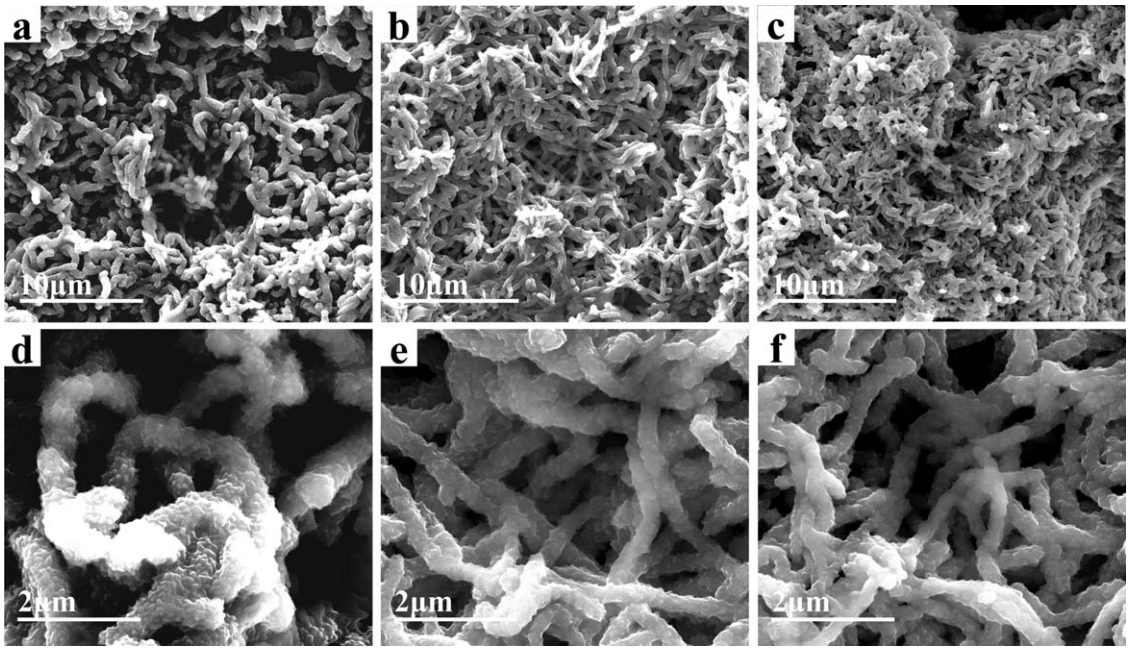

Figure 2. SEM images of PANI synthesized at various polymerization current densities: low magnification of (a) PANI-2, (b) PANI-6, (c) PANI-10, and high magnification of (d) PANI-2, (e) PANI-6, and (f) PANI-10, respectively.

FTIR Spectra Analysis

The FTIR absorption spectra of PANI synthesized at different current densities are shown in Figure 3. In the range of 900–1800 cm^{-1}, all samples have six major absorption bands located at ~1643, 1557, 1466, 1294, 1235, and 1062 cm^{-1}, which is in accordance with Kellenberger et al.'s results.[25] They are attributed to C═N stretching in quinoid ring (Q), C═C stretching in quinoid ring, C═C stretching in benzenoid ring (B), C—N stretching in QBB, BBQ, or QBQ, C—N stretching in BBB, and QNH^+B stretching, respectively. Among these bands, the intensity of QNH^+B stretching, assigned as characteristic band of emeraldine salt, is strongest. QNH^+B are formed via doping

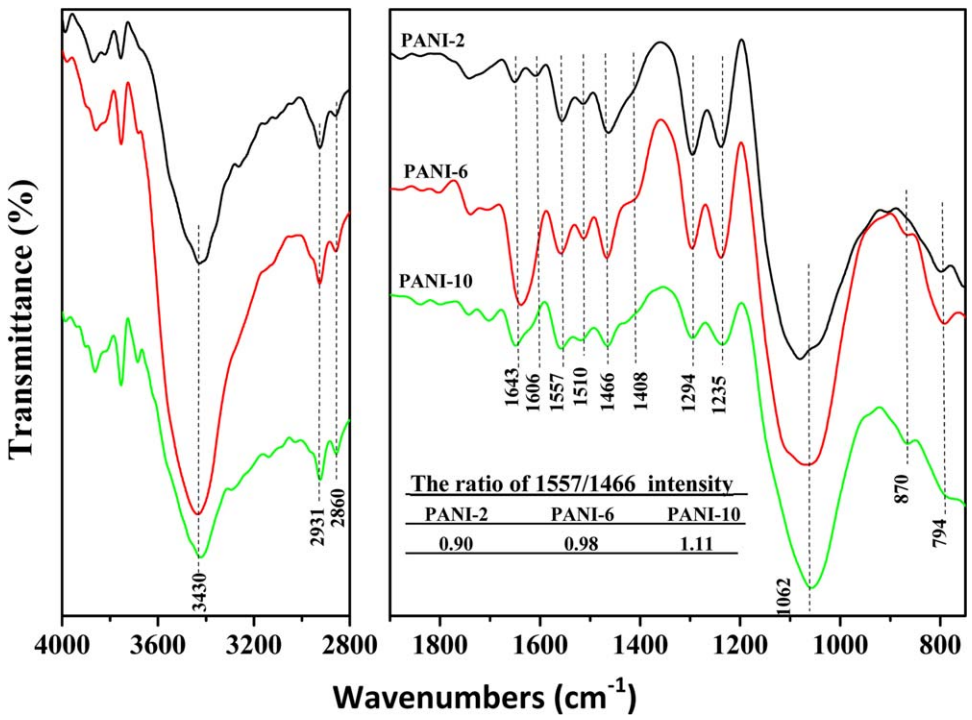

Figure 3. FTIR spectra of PANI samples synthesized at various current densities: PANI-2, PANI-6, and PANI-10; the ratio of 1557/1466 intensity is shown in the inset. [Color figure can be viewed in the online issue, which is available at wileyonlinelibrary.com.]

Table I. Analysis of Absorption Bands Appeared in FTIR Spectra of PANI

Wavenumbers	Assignment[a]
3430	υ (N—H)
2931	υ (C—H) in CH_3
2860	υ (C—H) in CH_2
1643	υ (C=N) in Q
1606	υ (C—C) in Q
1557	υ (C=C) in Q
1510	υ (C—C) in B
1466	υ (C=C) in B
1408	υ (C—N^+)
1294	υ (C—N) in QBB, BBQ, and QBQ
1235	υ (C—N) in BBB
1062	υ (QNH^+B)
870	γ (C—H) in 1,2,4 trisubstituted B
794	γ (C—H) in 1,4 disubstituted B

[a] υ, stretching mode; γ, out-of-plane bending mode; B, benzene ring; Q, quinoid ring.

PANI with H^+. They are usually considered as polaron or bipolaron which can form an excitation band between valence and conduction band. Hence, they play the key role in electrical conduction in PANI.[26,27] Among all specimens, the intensity of QNH^+B in PANI-6 is strongest, which reflects the concentration of polaron or bipolaron in PANI-6 is highest and there may be a greater chance for the higher conductivity of PANI-6. This point is also supported by the fact that the spectrum of PANI-6 exhibits highest intensity of a shoulder around 1400 cm^{-1} presumably corresponding to the hydrogen-bonded C—N^+ stretching.[28]

The bands posit at 1560 and 1465 cm^{-1} should also be paid more attention because their relative intensity can provide information on the DO of the polymer,[29–31] and hence we list the I_{1560}/I_{1465} in the inset of Figure 3. From the inset, we can see that the relative DO increases with polymerization current density. This can be explained that larger polymerization current density results in higher polymerization potential (Figure 1), which possesses stronger oxidizability and oxidizes more benzenoid rings to quinoid rings. These ratios are somewhat close to unity, indicating that PANI samples obtained in our experiments display an emeraldine form, which plays an important role in the heavily doped compositions and grant PANI the possibility of getting high conductivity.[32]

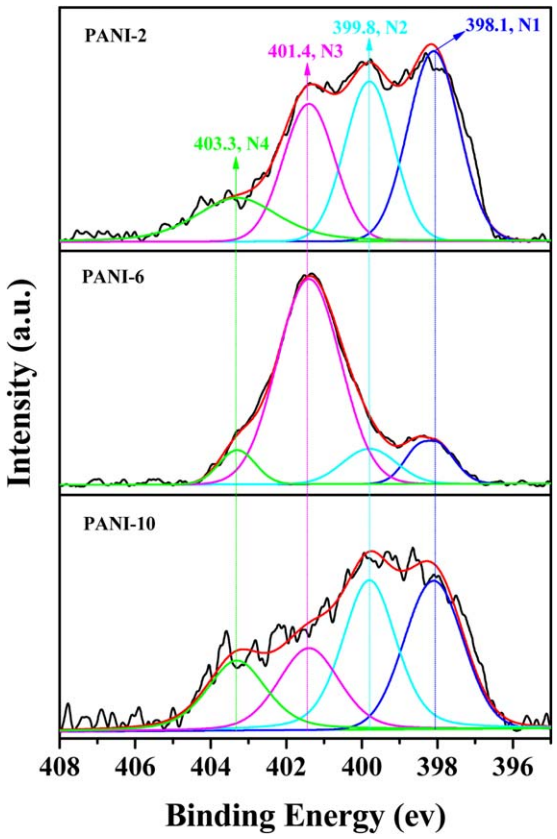

Figure 5. N1(s) XPS core-level spectra and deconvoluted plots of (a) PANI-2, (b) PANI-6, and (c) PANI-10. [Color figure can be viewed in the online issue, which is available at wileyonlinelibrary.com.]

The FTIR spectra show some bands in the range from 2800 to 4000 cm^{-1} caused by N—H stretching vibrations in the polymer structure and C—H stretching of CH_3 or CH_2. A summary of the analysis of absorption bands is provided in Table I, including their assignments based on Refs. 25,33,34.

Surface Elemental Chemical State

In the light of the previous studies,[35–38] it has turned out that PANI consists of four types of constitutional units: imino-1, 4-phenylene (IP), its salt, nitrilo-2 (IP^+), 5-cyclohexadiene-1, 4-diylidenenitrilo-1, 4-phenylene (NP), and radical cation of (IP^+) as shown in Figure 4. Hence, there are four kinds of nitrogen species in PANI chains, marked as N1, N2, N3, and N4. The N1s core level spectra, therefore, are deconvoluted into four components at binding energy of 398.1, 399.8, 401.4, and 403.3 ev as shown in Figure 5, corresponding to N1, N2, N3,

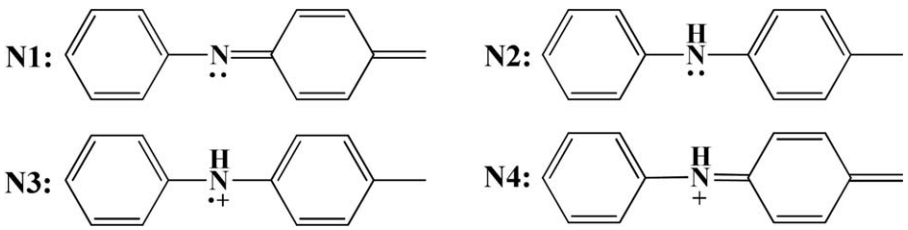

Figure 4. Constitutional units of PANI: N1, nitrilo-2,5-cyclohexadiene-1,4-diylidenenitrilo-1,4-phenylene; N2, imino-1,4-phenylene; N3, radical cation of imino-1, 4-phenylene; and N4, imino-1,4-phenylene salt.

Table II. Effect of Polymerization Current Density on the Relative Contents of the Various Nitrogen Species, DL

Sample	N1 (%) 398.1 (ev)	N2 (%) 399.8 (ev)	N3 (%) 401.4 (ev)	N4 (%) 403.3 (ev)	DL (%)
PANI-2	33.6	27.1	24.4	14.9	39.3
PANI-6	11.8	10.4	71.0	6.8	77.8
PANI-10	30.6	32.4	19.5	17.5	37.0

and N4, respectively. Their relative intensities are gained from the integrated intensities of the peaks. The contents of each nitrogen species are summarized in Table II.

It is well known that N3 and N4 are caused by doping polymer chain with $HClO_4$.[37] Hence, we can regard the sum of content of N3 and N4 as DL of PANI. As summarized in Table II, we can see that the DL of PANI-6 is the highest. It demonstrates that PANI synthesized at 6 mA cm^{-2} is facilely doped; higher or lower polymerization current density can give rise to a drop in DL. It is possible that the potential of doping is not comparable with that of generated by the current density of 2 or 10 mA cm^{-2}.

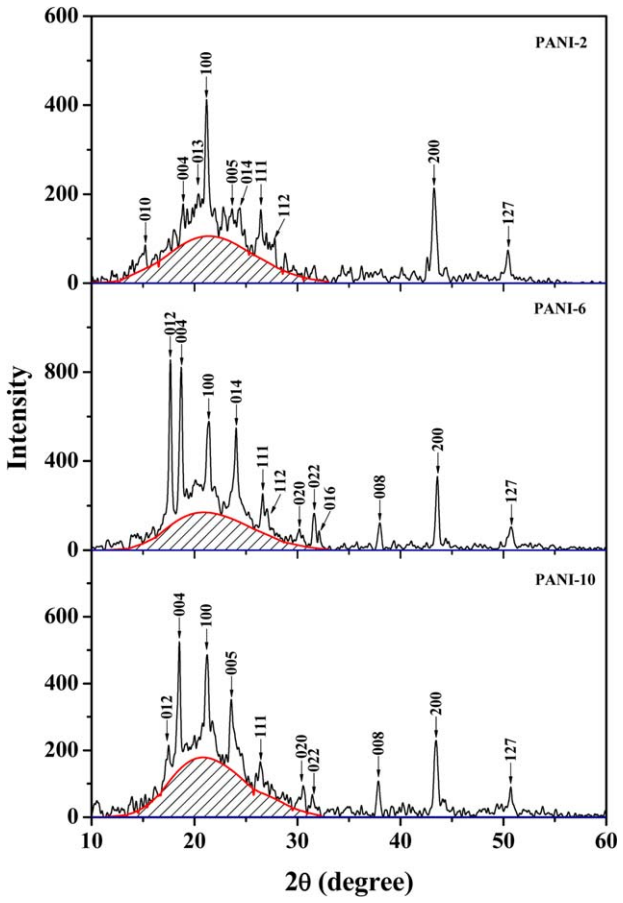

Figure 6. X-ray powder diffraction patterns of PANI-2, PANI-6, and PANI-10 (the contribution of amorphous part of the polymers used to calculate the crystallinity degree is outlined by hatching). [Color figure can be viewed in the online issue, which is available at wileyonlinelibrary.com.]

It is considered that N3 and N4 act as carriers during the course of electron transfer. Hence, the higher DL is, the more carriers are there, and the higher is the conductivity. N1s XPS core level analysis illustrates that DL of PANI-6 is greater by a factor of ~2 than that in PANI-2, which exceeds PANI-10 by a little. Hence, the conductivity of PANI-6 is expected to be best. This is satisfied with the results observed in FTIR spectra.

Crystalline Structure Studies

The powder XRD patterns of three kinds of PANI samples are shown in Figure 6 and the corresponding data are summarized in Table III. All the main reflections observed in patterns can be indexed in a pseudo-orthorhombic cell[14,15,39–41] and the results are also summarized in Table III. A least-square fit of their 2θ angular positions leads to the unit cell parameters as listed in Table IV. The experimentally observed lattice parameters are in good agreement with the reported values from Pouget.[14]

The crystalline domain size, L, can be estimated from the full width at half maximum (FWHM) using the Scherrer formula

$$L = \frac{0.89\lambda}{\beta \cos\theta} \tag{1}$$

where λ is the X-ray wavelength used, β is FWHM at Bragg angle 2θ. The L-values, associated with the strongest peak, are listed in Table IV. The crystalline coherence length of PANI-6 is the largest among all samples, which favors carriers transfer along the PANI chain and promotes the conductivity of PANI.

The interchain separation length (R) corresponding to the highest intense crystalline peak, determined from the relationship (see Formula 2) given by Klug and Alexander,[42] is also listed in Table IV.

$$R = \frac{5\lambda}{8 \sin\theta} \tag{2}$$

From the data summarized in Table IV, it is clear that PANI-2 has shortest R-value, which promotes its conductivity according to the fact that the probability of interchain hopping increases with the decrease in interchain separation.[18]

The values of crystallinity degree (X_{cr}) for these samples have been calculated from intensities corresponding to crystalline and amorphous reflexes, according to a series of formula as follows[43]:

$$X_{cr} = \frac{\sum_i C_{i,hkl}(\theta) I_{i,hkl}(\theta)}{\sum_i C_{i,hkl}(\theta) I_{i,hkl}(\theta) + \sum_j C_j(\theta) I_j(\theta) k_i} \times 100\% \tag{3}$$

where i, j is the number of crystalline and amorphous peaks, respectively. $C_{i,\ hkl}(\theta)$, $I_{i,\ hkl}(\theta)$ corresponds, respectively, to the

Table III. XRD Data of PANI Samples: Bragg Angle 2θ, Spacing d, and Indexation (hkl)

PANI-2		PANI-6		PANI-10		
2θ (°)	d (Å)	2θ (°)	d (Å)	2θ (°)	d (Å)	(hkl)
15.21	5.825					(010)
		17.66	5.023	17.48	5.073	(012)
18.89	4.697	18.71	4.743	18.53	4.789	(004)
20.38	4.358					(013)
21.17	4.197	21.40	4.153	21.23	4.186	(100)
23.66	3.761			23.57	3.775	(005)
24.40	3.648	24.04	3.702			(014)
26.45	3.370	26.63	3.347	26.41	3.375	(111)
27.79	3.210	27.05	3.297			(112)
		30.19	2.960	30.56	2.963	(020)
		31.62	2.830	31.44	2.846	(022)
		32.11	2.788			(016)
		38.00	2.368	37.85	2.377	(008)
43.30	2.090	43.59	2.076	43.47	2.082	(200)
50.45	1.809	50.75	1.799	50.72	1.800	(127)

Table IV. Unit Cell Parameters, Domain Length of the Strongest Peak L, Interchain Separation Length R, and Crystallinity Degree of PANI X_{cr}

	Lattice parameters (Å)						
Sample	a	b	c	Volume V (Å^3)	L (Å)	R (Å)	X_{cr} (%)
PANI-2	4.186	5.926	18.793	466	199	5.3	44.8
PANI-6	4.155	5.915	18.980	466	320	6.2	67.3
PANI-10	4.170	5.851	19.060	465	236	6.0	62.0

emendatory factor and integrated intensity of crystalline peak at (hkl) reflection. $C_j(\theta)$, $I_j(\theta)$ associates with the emendatory factor and integrated intensity of amorphous peak. k_i is the ratio of integrated intensity of crystalline peak used to calculate to that of whole crystalline peaks. The $C_{i,hkl}(\theta)$ and $C_j(\theta)$ are given by

$$C^{-1}(\theta)=f^2\times\frac{1+\cos^2 2\theta}{\sin^2\theta\cos\theta}\times e^{-10(\sin\theta/\lambda)^2}=\sum_i N_i f_i^2\times\frac{1+\cos^2 2\theta}{\sin^2\theta\cos\theta}\times e^{-10(\sin\theta/\lambda)^2} \quad (4)$$

where f represents the summation of all atoms scattering factors in one repeat unit. N_i, f_i is the number and the scattering factor of i atom one repeat unit contains, respectively. f_i is given by

Table V. The Electrical Conductivity of PANI Samples Synthesized at Different Current Densities

	PANI-2	PANI-6	PANI-10
Conductivity (S cm^{-1})	20.6	27.1	19.8

$$f_i(\sin\theta/\lambda)=\sum_{j=1}^{4} a_j\times e^{-2b_j(\sin\theta/\lambda)^2}+C \quad (5)$$

where a_j, b_j, and C can be obtained from Refs.[44,45] From the data summarized in Table IV, we can see that X_{cr} of PANI-6 is higher than any other samples. The reason may be that the effects of electric field are more benefit to the ordered arrangement of the polymer chain at 6 mA cm^{-2}. Thus, appropriate polymerization current density is useful for gaining higher order polymer. The higher crystalline order shows that there is a longer range order and coherence length in PANI chain. Pouget[14] has demonstrated that the metallic region is associated with the crystalline portion of the sample. Heffner and coworkers[46,47] consider that the order packing in the crystalline regions produces a high degree of local chain orientation and also reduces the energy required for interchain transport. Hence, such improvement in the order is benefit to the conductivity and charge transport processes.[48]

Electrical Conductivity

The room-temperature conductivities of PANI samples are summarized in Table V. The conductivity of PANI-6 is highest. As it is known, the room-temperature conductivity of the conjugated polymers is determined by a series of factors: carrier

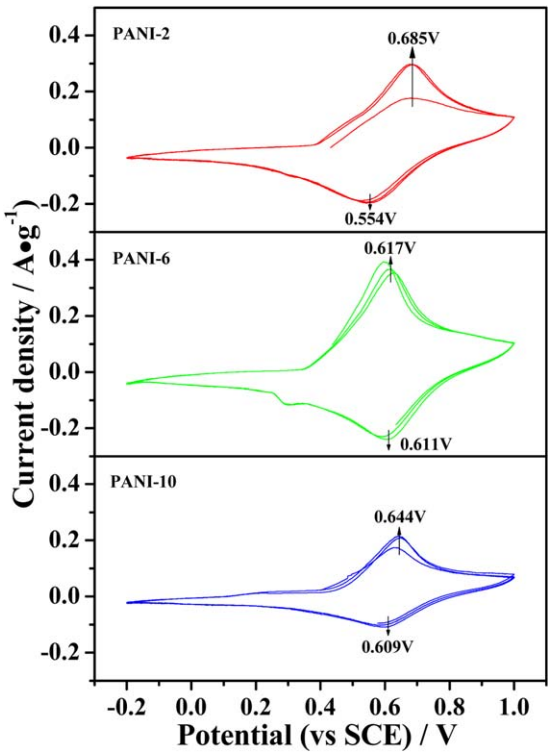

Figure 7. Cyclic voltammograms of PANI-2, PANI-6, and PANI-10 at a scan rate of 1 mv s^{-1}. [Color figure can be viewed in the online issue, which is available at wileyonlinelibrary.com.]

concentration, DO, DL, interchain separation length, as well as crystallinity.[40,49] According to the results of FTIR spectroscopy, PANI-6 has strongest $QNH^{+}B$ band, which indicates that there is highest concentration of carrier, including polaron and bipolaron. The DO of PANI-6 is more close to unity, which implies PANI-6 possesses perfect emeraldine structure. XPS analysis manifests that DL of PANI-6 is much higher than others. Furthermore, crystalline structure studies show that PANI-6 presents better order packing and longer domain length. As a comprehensive consideration of these results, we can obtain best conductivity of PANI when 6 mA cm^{-2} was loaded. The conductivity of PANI-2 is a little better than that of PANI-10, which possibly attributes to the shorter interchain separation length and the larger size of nanofibers in PANI-2.

CV Measurement

The CV curves of PANI samples at the scanning rate of 1 mV s^{-1} are shown in Figure 7. One couple of redox peaks (0.685/0.554 V for PANI-2, 0.617/0.611 V for PANI-6, and 0.644/0.609 V for PANI-10) appears in the CV curves, which is caused by the redox transitions of emeraldine/polaronic emeraldine form. The gap between anode and cathode peaks is 0.131, 0.006, and 0.035 V, respectively. It means, PANI-6 owns least polarization which profits electrochemical properties. In addition, current response and CV curve area of PANI-6 also exceed those of PANI-2 and PANI-10. The presented differences of the electrochemical characteristics among the analyzed PANI samples could be explained with the mentioned morphological features, structural characteristics, and conductivity: the enlarged specific surface area, enhanced ordering, increased carrier concentration, and improved conductivity of this polymer result in more reaction sites, less energy of ionic diffusion, greater discharge capacity, larger current peak in CV curve, and higher reversibility of redox processes taking place in the polymer during cycling of the potential.[11,40] Comparing to PANI-2, PANI-10 occupies less polarization mainly benefiting from its large specific surface area.

CONCLUSIONS

In this study, PANI with high crystallinity degree was successfully grown on the surface of stainless steel net via galvanostatic method. The analysis showed that the morphology, structure, and electrochemical properties changed a lot with increase in polymerization current density. PANI synthesized at a current density of 6 mA cm^{-2} possessed perfect emeraldine structure, leading to higher DL of 77.8% and carrier concentration. Meanwhile, this PANI sample presented better packing of the chains in polymer matrix, much higher crystallinity degree of 67%, and larger crystalline domain size. In addition, PANI-6 owned high specific surface area. Consequently, PANI-6 exhibited great conductivity (27.1 S cm^{-1}), discharge capacity, and reversibility. This kind of PANI can be regarded as a promising electrode in the application of supercapacitor and lithium ion battery.

ACKNOWLEDGMENTS

This investigation was supported by the National Natural Science Foundation of China (Grant No. 50902109 and 51201128), the Natural Science Foundation of Shaanxi Province (Grant No. 2010JQ6002), and the Fundamental Research Funds for the Central Universities (Grant No. XJJ2012076). The authors also gratefully acknowledge Miss Yanzhu Dai and Mr. Liang Li for help in SEM.

REFERENCES

1. Lee, K.; Cho, S.; Park, S. H.; Heeger, A. J.; Lee, C. W.; Lee, S. H. *Nature* **2006**, *441*, 65.
2. Huang, W. S.; Macdiarmid, A. G. *Polymer* **1993**, *34*, 1833.
3. Yao, Q.; Chen, L.; Zhang, W.; Liufu, S.; Chen, X. *ACS Nano* **2010**, *4*, 2445.
4. Wang, Y.-G.; Li, H.-Q.; Xia, Y.-Y. *Adv. Mater.* **2006**, *18*, 2619.
5. Ryu, K. S.; Kim, K. M.; Kang, S. G.; Lee, G. J.; Joo, J.; Chang, S. H. *Syn. Met.* **2000**, *110*, 213.
6. Cao, Y.; Andreatta, A.; Heeger, A. J.; Smith, P. *Polymer* **1989**, *30*, 2305.
7. Okamoto, H.; Kotaka, T. *Polymer* **1998**, *39*, 4349.
8. Okamoto, H.; Okamoto, M.; Kotaka, T. *Polymer* **1998**, *39*, 4359.
9. Sazou, D.; Kourouzidou, M.; Pavlidou, E. *Electrochim. Acta* **2007**, *52*, 4385.
10. Guo, Y.; Zhou, Y. *Eur. Polym. J.* **2007**, *43*, 2292.
11. Shaolin, M.; Yifei, Y. *J. Phys. Chem. B* **2008**, *112*, 11558.
12. Xing-Rong, Z.; Tze-Man, K. *Polymer* **1998**, *39*, 1187.

13. Holze, R.; Stejskal, J. *Chem. Pap.* **2013**, *67*, 769.
14. Pouget, J. P.; Jozefowicz, M. E.; Epstein, A. J.; Tang, X.; Macdiarmid, A. G. *Macromolecules* **1991**, *24*, 779.
15. Jozefowicz, M. E.; Epstein, A. J.; Pouget, J. P.; Masters, J. G.; Ray, A.; Macdiarmid, A. G. *Macromolecules* **1991**, *24*, 5863.
16. Maron, J.; Winokur, M. J.; Mattes, B. R. *Macromolecules* **1995**, *28*, 4475.
17. Bhadra, S.; Khastgir, D. *Polym. Test.* **2008**, *27*, 851.
18. Bhadra, S.; Lee, J. H. *J. Appl. Polym. Sci.* **2009**, *114*, 331.
19. Bhadra, S.; Kim, N. H.; Lee, J. H. *J. Appl. Polym. Sci.* **2010**, *117*, 2025.
20. Ren, Y. J.; Zeng, C. L. *J. Power Sources* **2008**, *182*, 524.
21. Genies, E. M.; Tsintavis, C. *J. Electroanal. Chem.* **1985**, *195*, 109.
22. Zotti, G.; Cattarin, S.; Comisso, N. *J. Electroanal. Chem.* **1988**, *239*, 387.
23. Wen, J. B.; Zhou, H. H.; Li, S. L.; Luo, S. L.; Chen, J. H.; Kuang, Y. F. *Acta Phys. Chim. Sin.* **2006**, *22*, 106.
24. Mehdinla, A.; Mousavi, M. F. *J. Sep. Sci.* **2008**, *31*, 3565.
25. Kellenberger, A.; Dmitrieva, E.; Dunsch, L. *J. Phys. Chem. B* **2012**, *116*, 4377.
26. Su, W. P.; Schrieffer, J. R.; Heeger, A. *J. Phys. Rev. Lett.* **1979**, *42*, 1698.
27. McCall, R. P.; Ginder, J. M.; Roe, M. G.; Asturias, G. E.; Scherr, E. M.; Macdiarmid, A. G.; Epstein, A. *J. Phys. Rev. B* **1989**, *39*, 10174.
28. Konyushenko, E. N.; Stejskal, J.; Trchova, M.; Hradil, J.; Kovarova, J.; Prokes, J.; Cieslar, M.; Hwang, J.-Y.; Chen, K.-H.; Sapurina, I. *Polymer* **2006**, *47*, 5715.
29. Quillard, S.; Louarn, G.; Lefrant, S.; Macdiarmid, A. G. *Phys. Rev. B* **1994**, *50*, 12496.
30. Man, J.; Shibu, Z.; Zuowan, Z.; An, Z.; Jun, L. *J. Appl. Polym. Sci.* **2011**, *121*, 3439.
31. Zhu, D.; Zhang, J.; Xu, C.; Matsuo, M. *Synth. Met.* **2011**, *161*, 1820.
32. Nechtschein, M.; Genoud, F.; Menardo, C.; Mizoguchi, K.; Travers, J. P.; Villeret, B. *Synth. Met.* **1989**, *29*, 211.
33. Laslau, C.; Ingham, B.; Zujovic, Z. D.; Capkova, P.; Stejskal, J.; Trchova, M.; Travas-Sejdic, J. *Synth. Met.* **2012**, *161*, 2739.
34. Hussain, A. A.; Sharma, S.; Pal, A. R.; Bailung, H.; Chutia, J.; Patil, D. S. *Plasma Chem. Plasma Process.* **2012**, *32*, 817.
35. Furukawa, Y.; Ueda, F.; Hyodo, Y.; Harada, I.; Nakajima, T.; Kawagoe, T. *Macromolecules* **1988**, *21*, 1297.
36. Nakajima, T.; Harada, M.; Osawa, R.; Kawagoe, T.; Furukawa, Y.; Harada, I. *Macromolecules* **1989**, *22*, 2644.
37. Monkman, A. P.; Stevens, G. C.; Bloor, D. *J. Phys. D Appl. Phys.* **1991**, *24*, 738.
38. Li, Y.; Yu, Y.; Wu, L.; Zhi, J. *Appl. Surf. Sci.* **2013**, *273*, 135.
39. Petkov, V.; Parvanov, V.; Trikalitis, P.; Malliakas, C.; Vogt, T.; Kanatzidis, M. G. *J. Am. Chem. Soc.* **2005**, *127*, 8805.
40. Posudievsky, O. Y.; Goncharuk, O. A.; Barille, R.; Pokhodenko, V. D. *Synth. Met.* **2010**, *160*, 462.
41. Souza, F. G., Jr.; Orlando, M. T. D.; Michel, R. C.; Pinto, J. C.; Cosme, T.; Oliveira, G. E. *J. Appl. Polym. Sci.* **2011**, *119*, 2666.
42. Klug, H. P.; Alexander, L. E. X-Ray Diffraction Procedures: For Polycrystalline and Amorphous Materials, 2nd ed.; Wiley-VCH: New York, May **1974**.
43. Mo, Z.; Zhang, H. Structure of Crystalline Polymers by X-Ray Diffraction; Science Press: Beijing, **2010**.
44. Cromer, D. T.; Waber, J. T. *Acta Crystallogr.* **1965**, *18*, 104.
45. Cromer, D. T.; Mann, J. B. Acta Crystallogr. Sect. A: Cryst. Phys. Diffr. Theor. Gen. *Crystallogr.* **1968**, *A24*, 321.
46. Pearson, D. S.; Pincus, P. A.; Heffner, G. W.; Dahman, S. *J. Macromolecules* **1993**, *26*, 1570.
47. Heffner, G. W.; Dahman, S. J.; Pearson, D. S.; Gettinger, C. L. *Polymer* **1993**, *34*, 3155.
48. Mani, A.; Athinarayanasamy, K.; Kamaraj, P.; Selvan, S. T.; Ravichandran, S.; Phani, K. L. N.; Pitchumani, S. *J. Mater. Sci. Lett.* **1995**, *14*, 1594.
49. Bhadra, S.; Khastgir, D.; Singha, N. K.; Lee, J. H. *Prog. Polym. Sci.* **2009**, *34*, 783.